Compressibility and crystal structure of andalusite at high pressure

RUSSELL L. RALPH

Department of Geological Sciences, University of Washington
Seattle, Washington 98195

LARRY W. FINGER, ROBERT M. HAZEN

Geophysical Laboratory, Carnegie Institution of Washington
Washington, D. C. 20008

AND SUBRATA GHOSE

Department of Geological Sciences, University of Washington
Seattle, Washington 98195

Abstract

The unit-cell dimensions and crystal structure of andalusite Al_2SiO_5 have been refined from X-ray data on single crystals mounted in a diamond anvil cell at pressures of 12, 25, and 37 kbar. Structure refinements with anisotropic temperature factors yielded weighted *R* factors of 3.4, 4.9, and 5.2% respectively. The bulk modulus of andalusite is 1.35 ± 0.10 mbar and the axial compression ratios of orthorhombic unit-cell axes $a:b:c$ are approximately $2.1:1.5:1.0$. The relatively greater compressibility of the $Al(1)-O_D$ bond results in a being the most compressible axis. Those bonds that compress $>3\sigma$ between 1 bar and 37 kbar at room temperature, are the bonds that also expand significantly between 25 and 1000°C at room pressure. Polyhedral bulk moduli for the Al(1) octahedron, the Al(2) trigonal bipyramid and the Si tetrahedron are 1.3 ± 0.2, 1.6 ± 0.5, and 4.1 ± 1.5 mbar, respectively. Thus, the aluminum polyhedra are significantly more compressible than the silicon tetrahedron. The omega step-scanning technique of X-ray intensity data collection results in a significant improvement in accuracy and is recommended for structure determination with the diamond-anvil high-pressure cell.

Introduction

High pressure structure determination contain valuable data on the equations of state, interatomic forces and chemical bonding in minerals. The Al_2SiO_5 polymorphs, andalusite, sillimanite and kyanite, provide an interesting system where aluminum occurs in three types of coordinations; in addition to the octahedral coordination found in all three minerals, aluminum also occurs in tetrahedal coordination in sillimanite and in five-fold trigonal bipyramidal coordination in andalusite. Knowledge of the response to pressure and temperature of these different types of Al–O bonds in the presence of relatively rigid SiO_4 tetrahedra is necessary for an understanding of the stability relations and phase transformation within the Al_2SiO_5 system. The temperature effects on the crystal structures of andalusite, sillimanite and kyanite have been determined by Winter and Ghose (1979). The elastic constants of andalusite and sillimanite have been determined by Vaughan and Weidner (1978), who used the Brillouin scattering technique. From infrared and Raman spectroscopic data, the phonon spectra of andalusite and their temperature dependence have been determined and interpreted on the basis of a rigid-ion model by Iishi et al. (1979).

In this paper are presented data on the high pressure structural response of andalusite to 37 kbar, as well as correlations between high-pressure changes and high-temperature response, elasticity, and phonon spectra. It has been possible to observe directly the structural elements of andalusite that are responsible for the compressibility and, hence, the elastic constants. The present data on andalusite at high-pressure, combined with high-temperature data of Winter and Ghose (1979), may be used to test the inverse relationship between structural responses due to temperature versus pressure (Hazen and Finger, 1982). Andalusite is a light-atom structure with a small unit-cell and orthorhombic symmetry and thus also constitutes a test case for the improvement in accuracy of X-ray intensity data collected at high pressure by the omega step-scanning technique. The resulting improvement in

the data resulted in a successful refinement of the anisotropic temperature factors in a complicated silicate structure at high pressure.

Experimental

A fragment of a gem-quality andalusite crystal from Minas Gerais, Brazil, (from the same sample used by Winter and Ghose (1979) for their high-temperature experiments) was used for high-pressure study. A square crystal plate approximately $100 \times 100 \times 50$ μm was selected and mounted along with small ruby chips in a diamond-anvil high-pressure cell of the Merrill–Bassett type (Merrill and Bassett, 1974) modified by Hazen and Finger (1977). The pressure medium was a 4:1 methanol:ethanol mixture. The ruby fragments were used for the pressure calibration by the R_1 ruby flourescence technique. The andalusite crystal was mounted with its (001) plane approximately parallel to the diamond faces and was secured with a small dot of petroleum jelly.

The first data set at 37 kbar was collected at the University of Washington on the Syntex $P\bar{1}$ four-circle automatic diffractometer with the $\theta-2\theta$ technique and Mo$K\alpha$ radiation monochromatized by reflecting from a graphite "single" crystal. All other data sets were collected at the Geophysical Laboratory on an automated four-circle diffractometer and Nb-filtered Mo$K\alpha$ radiation. All accessible reflections for which $\sin \theta/\lambda < 0.70$ were collected. The data were corrected for specimen and diamond-cell absorption as well as Lorentz and polarization factors. Results of unit-cell refinements at the pressures studied are shown in Table 1.

Data at 12 kbar were collected first with continuous omega scans and background measurements were determined from the intensities at the extremes of the scan. (Omega scans are necessary in diamond-cell studies because beryllium, which is used to support the diamonds, produces powder rings that interfere with $\theta-2\theta$ scans.) Data from symmetrically equivalent reflections were averaged prior to least-squares refinement with the program RFINE4 (Finger and Prince, 1975). Neutral scattering factors of Cromer and Mann (1968) and coefficients for anomalous scattering from Cromer and Liberman (1970) were used for all atoms. Refinement of a model with anisotropic atoms (46 parameters, including scale factor, extinction parameter, 14 positional and 30 thermal parameters), based on 380 observed averaged reflections ($I > 2 \sigma$) yielded a weighted R factor of 4.3% (7.2% unweighted).

Intensity data for andalusite at 12 kbar were recollected with stepwise omega scans (4 second counts at 0.025° intervals). Step-scan data were processed and displayed visually on a graphics CRT for each reflection; background positions were selected by the technique of Lehman and Larsen (1974), but could be
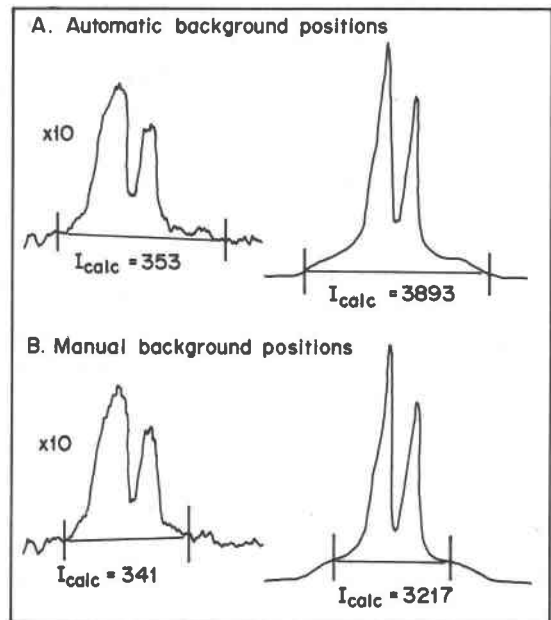

Fig. 1. Comparison of manual and automated background selection for evaluation of integrated X-ray intensities: (a) continuous omega scan, automatic background selection; (b) omega step-scan, manual background selection. Integrated intensities for weak reflections are similar with both procedures, but strong reflections, which may have white radiation shoulders, are often overestimated with automatic background selection.

modified manually prior to integration. Reflections were again corrected for absorption, and symmetrically equivalent reflections were averaged. Refinement based on 312 observed data from the step-scan procedure yielded a significantly improved anisotropic model, with a weighted R factor of 3.4% (3.4% unweighted).

Off-line selection of background positions, as facilitated by omega step-scan data collection, is an improvement over automated background collection for at least two reasons. When β-filtered radiation is used with a moving-crystal fixed counter technique, shoulders of intensity are observed in the vicinity of the Bragg peak (Fig. 1). As the crystal is rotated away from the

Table 1. Unit-cell parameters of andalusite

	1 bar*	12 kbar	25 kbar	37 kbar
a(Å)	7.7980(7)	7.7599(18)	7.7382(10)	7.7049(6)
b(Å)	7.9031(10)	7.8735(17)	7.8571(24)	7.8375(16)
c(Å)	5.5566(5)	5.5440(17)	5.5338(40)	5.5262(13)
V(Å³)	342.45(6)	338.72(15)	336.46(27)	333.71(11)

* From Winter and Ghose (1979)

Table 2. Refinement conditions and refined extinction parameters for andalusite at high pressure

	12 kbar Continuous	12 kbar Step-Scan	25 kbar Step-Scan	37 kbar Continuous
Number of observations $I > 2\sigma$	380	312	287	361
Weighted $\underline{R}$(%) [†]	4.3	3.4	4.9	5.2
$\underline{R}$(%) [††]	7.2	3.4	6.2	5.4
I^* ($\times 10^5$)	1.0(3)	2.8(4)	1.4(4)	0.8(3)

[†] Weighted $\underline{R} = [\Sigma w(F_o - F_c)^2/\Sigma wF_o^2]^{1/2}$

[††] $\underline{R} = \Sigma ||F_o| - |F_c|| / \Sigma |F_o|$

Parenthesized figures represent esd's.

Bragg position, the white radiation from the tube is diffracted into the counter first. Eventually the limits of the counter aperture are reached and the only radiation observed is general scattered radiation. Usually the scan limits are chosen to be large in order to reduce sensitivity to small shifts in crystal orientation; thus backgrounds are measured outside the shoulder regions. For weak reflections there is little difference in the intensities measured with continuous versus step-scan procedures. The effect is significant for a strong reflection for which the measured intensity is too large for continuous scan methods. In the refinement process, however, the scale factor and the tempera-

ture factors are adjusted in such a way that the discrepancies for strong reflections are minimized at the expense of weaker ones. As a result, the effect on unweighted R is much greater than for weighted R.

A second advantage to manual selection of background positions is the opportunity to view the shape of each peak in detail. Anomalies in peak shape due to diamond or ruby diffraction or other interference, are quickly identified and those aberrant reflections may be rejected from the data set prior to refinement.

Subsequent refinements of andalusite at 25 kbar employed the omega step-scan procedure for data collection. Refinement conditions and refined extinction parameters for andalusite appear in Table 2. Refined positional and thermal parameters appear in Table 3, while observed and calculated structure factors for four sets of andalusite intensity data appear in Tables 4a to 4d.[1]

[1] To obtain a copy of Tables 4a to 4d, order Document Am-84-239 from the Business Office, Mineralogical Society of America, 2000 Florida Avenue, N.W., Washington, D.C. 20009. Please remit $5.00 in advance for the microfiche.

Table 3. Refined positional and thermal parameters for andalusite

	1 bar[1]	12 kbar continuous	12 kbar step-scan	25 kbar step-scan	37 kbar Continuous
Al(1)					
x	0	0	0	0	0
y	0	0	0	0	0
z	.2419(1)	.2414(6)	.2416(5)	.2419(7)	.2414(5)
β_{11}	.0021(1)	.0031(3)	.0026(2)	.0036(4)	.0029(3)
β_{22}	.0029(1)	.0020(2)	.0017(2)	.0026(4)	.0018(3)
β_{33}	.0023(2)	.0058(12)	.0035(9)	.0007(15)	.0013(12)
β_{12}	.0005(11)	.0004(2)	.0004(2)	.0009(2)	.0001(2)
β_{13}	0	0	0	0	0
β_{23}	0	0	0	0	0
B_{eq}	.46(2)	.65(4)	.49(4)	.53(6)	.42(5)
Al(2)					
x	.3705(1)	.3593(3)	.3702(2)	.3702(3)	.3699(2)
y	.1391(1)	.1390(2)	.1391(2)	.1386(3)	.1387(2)
z	.5	.5	.5	.5	.5
β_{11}	.0009(1)	.0022(3)	.0014(2)	.0022(3)	.0016(2)
β_{22}	.0026(1)	.0019(3)	.0015(2)	.0020(4)	.0020(3)
β_{33}	.0028(2)	.0054(13)	.0046(9)	.0052(15)	.0022(11)
β_{12}	.0000(1)	.0001(3)	-.0003(2)	-.0003(3)	.0004(2)
β_{13}	0	0	0	0	0
β_{23}	0	0	0	0	0
$B_{eq.}$	.34(2)	.55(5)	.42(4)	.55(6)	.38(5)
Si					
x	.2460(1)	.2461(3)	.2459(2)	.2460(3)	.2467(2)
y	.2520(1)	.2515(3)	.2514(2)	.2505(3)	.2500(2)
z	0	0	0	0	0
β_{11}	.0007(1)	.0019(2)	.0015(2)	.0019(3)	.0012(2)
β_{22}	.0024(1)	.0020(2)	.0012(2)	.0019(3)	.0015(2)
β_{33}	.0025(2)	.0041(10)	.0041(8)	.0047(14)	.0050(11)
β_{12}	.0000(1)	.0002(2)	-.0002(1)	.0000(2)	.0001(1)
β_{13}	0	0	0	0	0
β_{23}	0	0	0	0	0
$B_{eq.}$	.31(2)	.49(4)	.39(3)	.51(5)	.42(4)
O_A					
x	.4233(2)	.4222(5)	.4221(4)	.4220(7)	.4203(5)
y	.3629(2)	.3631(6)	.3634(4)	.3632(8)	.3639(5)
z	.5	.5	.5	.5	.5
β_{11}	.0018(2)	.0034(7)	.0024(5)	.0025(8)	.0024(5)
β_{22}	.0028(2)	.0016(7)	.0021(5)	.0027(9)	.0019(6)
β_{33}	.0030(4)	.0059(29)	.0009(22)	.0066(36)	.0027(5)
β_{12}	-.0003(2)	-.0001(6)	-.0003.(4)	.0004(7)	-.0011(5)
β_{13}	0	0	0	0	0
β_{23}	0	0	0	0	0
$B_{eq.}$	.46(5)	.64(10)	.41(8)	.69(13)	0

Table 3. (continued)

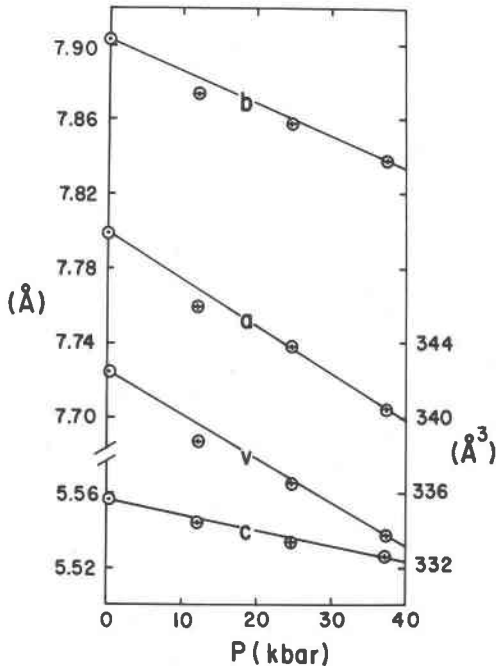|	1 bar[1]	12 kbar continuous	12 kbar step-scan	25 kbar step-scan	37 kbar Continuous
O_B					
x	.4246(2)	.4247(5)	.4249(4)	.4260(7)	.4269(5)
y	.3629(2)	.3621(6)	.3623(5)	.3608(8)	.3598(6)
z	0	0	0	0	0
β_{11}	.0011(2)	.0030(7)	.0026(5)	.0025(7)	.0027(5)
β_{22}	.0031(2)	.0022(7)	.0020(5)	.0035(9)	.0021(6)
β_{33}	.0031(4)	.0060(29)	.0026(22)	.0017(37)	.0037(28)
β_{12}	-.0006(2)	-.0005(6)	.0007(4)	-.0009(7)	-.0002(5)
β_{13}	0	0	0	0	0
β_{23}	0	0	0	0	0
$B_{eq.}$	.44(5)	.67(10)	.48(8)	.56(13)	.45(9)
O_C					
x	.1030(2)	.1034(6)	.1031(4)	.1031(7)	.1034(5)
y	.4003(2)	.4004(5)	.4000(4)	.3999(7)	.4008(5)
z	0	0	0	0	0
β_{11}	.0010(2)	.0018(7)	.0015(5)	.0036(8)	.0021(5)
β_{22}	.0027(2)	.0027(7)	.0013(5)	.0025(9)	.0010(6)
β_{33}	.0086(5)	.0059(28)	.0066(22)	.0068(37)	.0065(29)
β_{12}	.0002(2)	.0001(5)	-.0003(4)	-.0012(7)	.0001(4)
β_{13}	0	0	0	0	0
β_{23}	0	0	0	0	0
$B_{eq.}$	.60(5)	.61(10)	.51(8)	.78(13)	.51(10)
O_D					
x	.2305(2)	.2298(3)	.2303(3)	.2303(5)	.2296(3)
y	.1339(2)	.1337(4)	.1327(3)	.1324(5)	.1308(4)
z	.2394(2)	.2389(8)	.2389(6)	.2387(9)	.2399(7)
β_{11}	.0016(2)	.0024(4)	.0025(4)	.0030(6)	.0024(4)
β_{22}	.0032(2)	.0032(4)	.0018(3)	.0030(7)	.0020(4)
β_{33}	.0030(3)	.0036(22)	.0045(16)	.0017(29)	.0033(2)
β_{12}	-.0004(1)	-.0005(4)	.0000(3)	-.0004(8)	-.0003(3)
β_{13}	-.0004(1)	-.0001(7)	-.0007(5)	-.0003(8)	-.0010(6)
β_{23}	.0005(2)	.0002(7)	.0010(5)	.0000(7)	.0010(5)
$B_{eq.}$	.49(3)	.61(8)	.54(6)	.55(10)	.49(7)

[1]From Winter and Ghose (1979).

Fig. 2. Variations of the unit cell dimensions and volume with pressure. The error bars (one standard deviation) are indicated in terms of crosses.

Results

Unit-cell parameters

All three unit-cell dimensions decrease with pressure (Fig. 2). The data points at 1 atmosphere are from Winter and Ghose (1979). The compressibility of andalusite is strongly anisotropic; the coefficients of linear compression ($\beta l = \triangle l / l \triangle p$) for three unit-cell axes are 3.2±0.4, 2.2±0.4, and 1.5±0.5 × 10^{-4} kbar^{-1} for β_a, β_b and β_c respectively. Axial compression ratios for $a:b:c$ are thus 2.1:1.5:1.0. The bulk modulus of andalusite obtained for a Birch-Murnaghan equation of state (K' = 4) is 1.39±0.10 mbar.

Structural changes at high pressure

Andalusite is orthorhombic, space group *Pnnm*, with four Al_2SiO_5 units in the unit cell. The crystal structure of andalusite consists of tetragonally distorted Al(1) octahedra sharing edges to form chains along the c-axis. These chains are located at the corners and the middle of the unit cell, the orientation of the long octahedral axes (direction of the Al(1)–O_D bond) being approximately 30° to the left and right of the **a** axis. These octahedral chains are linked through SiO_4 tetrahedra and edge-sharing pairs of Al(2)-trigonal bipyramids (Taylor, 1929; Burnham and Buerger, 1961) (Fig. 3). Under pressures up to 37 kbar, no phase transitions or changes in structural topology are observed, but several significant changes in bond distances are evident.

Within the Al(1) octahedron, the long Al(1)–O_D bond length decreases most with pressure (1.97% at 37 kbar), the intermediate bond Al(1)–O_B remains unchanged, and the shortest Al(1)–O_A bond decreases slightly (0.66% at 37 kbar). Hence, the compressibility of a bond length is not necessarily always a direct function of magnitude. A similar behavior is reflected at high temperature, where the Al(1)–O_D bond increases the most, the Al(1)–O_B bond remains unchanged and the Al(1)–O_A bond increases slightly (Winter and Ghose, 1979). At pressure the average (Al(1)–O bond length changes from 1.935Å at 1 bar to 1.916Å at 37 kbar and the octahedral volume correspondingly changes from 9.538 to 9.281Å^3.

Within the Al(2) trigonal bipyramid, all of the bond lengths decrease with pressure, the longest Al(2)–O_C bond decreasing the most. Winter and Ghose (1979) observed this bond to increase the most with temperature. With pressure, however, the difference in Al(2)–O bond lengths decreases only slightly, and there is no significant change in O–Al(2)–O bond angles. Hence, for the Al(2) polyhedron, no tendency to become more regular is observed at high pressure.

Within the SiO_4 tetrahedron, the longest Si–O bond, Si–O_B, decreases from 1.645Å at 1 bar to 1.633Å at 37 kbar, which is significant. In contrast, the shorter Si–O_C and Si–O_D bonds do not show any decrease with pressure. Shortening of Si–O bonds has also been observed in diopside by Levien and Prewitt (1981). At high temperature, the Si–O_B bond in andalusite is observed to increase slightly from 1.645(4)Å at room temperature to 1.650(2)Å at 1000°C (Winter and Ghose, 1979). In view of the fact that the thermal vibrations at high temperature result in a
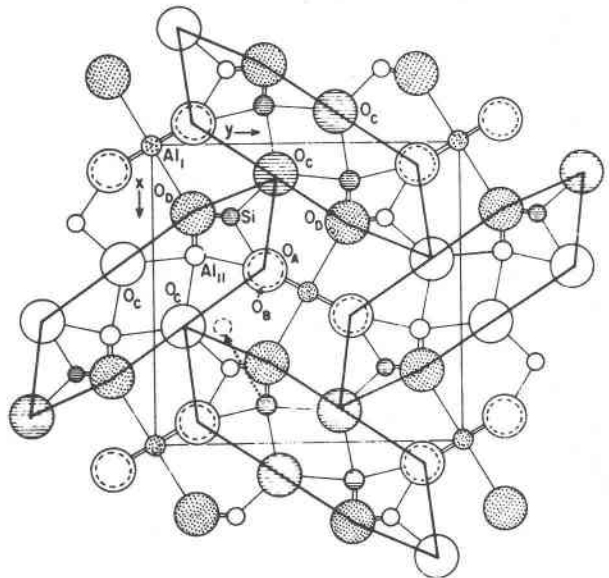

Fig. 3. Projection of the andalusite crystal structure on (001) after Burnham and Buerger, 1961). Atoms are represented by striped circles at z = 0, stippled circles at z = 1/4, and clear circles at z = 1/2. Chains of Si and Al(2) polyhedra are outlined.
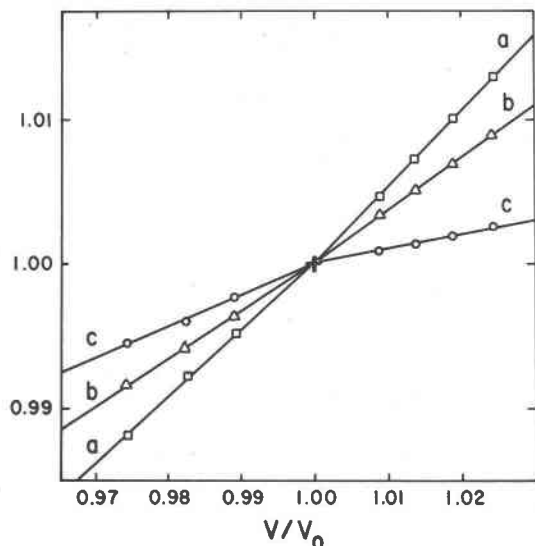
Fig. 4. Plot of unit cell l/l_0 versus V/V_0 demonstrate that axial variations are similar for temperature and pressure changes. High-temperature data are from Winter and Ghose (1979).

lower value of the Si–O bond length than its true value, the small increase of the Si–O_B bond length with temperature may be significant and in accord with shortening of this bond at high pressure.

Discussion

Inverse relationship between pressure and temperature effects

When the unit-cell dimensions and bond lengths (X) normalized with respect to X_0 under ambient conditions are plotted against V/V_0, where V_0 is the unit-cell volume at room temperature and pressure, a roughly inverse behavior is commonly observed. As Levien and Prewitt (1981) have shown in the case of diopside, however, this relationship does not strictly hold because of the different response of the structure to pressure and temperature. In andalusite a similar behavior is observed. Among the unit-cell dimensions, c deviates most strongly from such inverse behavior (Fig. 4). In terms of the long Al(1)–O_D bond, which compresses the most, a strictly inverse behavior is also not observed (Fig. 5). This observation is not surprising in view of the fact that at high temperature, the anharmonic thermal vibrations of the atoms increase considerably. It is this effect that may explain the non-reciprocity of the P and T response of the silicate structures.

The elasticity of andalusite: relationship with thermal expansion and compressibility.

The elastic constants of andalusite have been measured by the Brillouin scattering technique by Vaughan and Weidner (1978). The principal elastic constants:

$c_{11}:2.334$, $c_{22}:2.890$ and $c_{33}:3.801$ mbar have been correlated with the crystal structure by the authors, who suggest that the Al(1) octahedra control the elasticity in these directions, and thus are more compliant than the lower-coordinated polyhedra. The data on thermal expansion and compressibility are in accord with the measured elastic constants $c_{11} < c_{22} < c_{33}$.

The andalusite structure is most compressible along the **a**-axis and least compressible along the **c**-axis. This effect is principally the result of compression of the long Al(1)–O_D bond, which lies on the **ab**-plane at 30° to the **a**-axis. A similar interpretation of the thermal expansion in andalusite has already been offered by Winter and Ghose (1979). The intermediate compressibility along the **b**-axis is most likely a consequence of the compression of the long Al(2)–O_C bond, which lies parallel to the **b**-axis. The bulk modulus measured from static compressibility data (1.39 mbar) is in agreement with the zero pressure value of 1.33 mbar obtained by Brace et al. (1969), but not with the Reuss bound value (1.580 mbar) of Vaughan and Weidner (1978). The correction between isothermal and adiabatic moduli (Anderson, 1966) is on the order of 0.1% and is too small to explain this discrepancy.

Polyhedral bulk-moduli in andalusite

The observed bulk moduli for the Al(1) octahedron, Al(2) trigonal bipyramid and the SiO_4 tetrahedron are 1.3 ± 0.2, 1.6 ± 0.5 and 4.1 ± 1.5 mbar respectively. These values are considerably less than those predicted from the linear bulk modulus–polyhedral volume relationship,
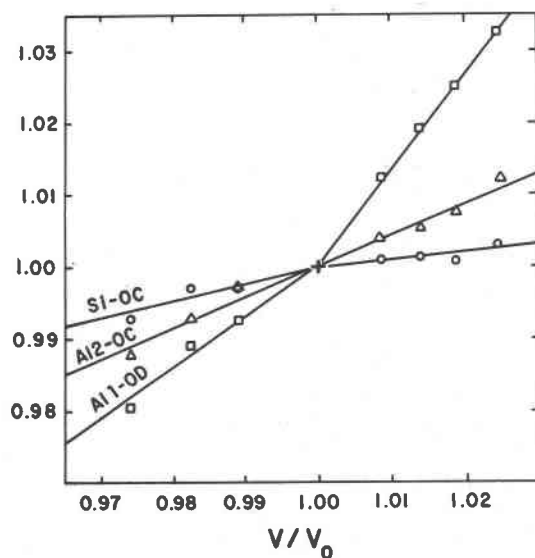

Fig. 5. Plots of bond distance d/d_0 versus unit cell V/V_0 for the longest bond in each of the three cation polyhedra of andalusite. High-temperature structural variations mirror approximately those at high pressure; but the change of slope at the origin indicates that the "inverse relationship" is not exact. High temperature data from Winter and Ghose (1979).

Table 5. Selected interatomic distances and angles for andalusite

Bond Lengths (Å)	1 bar[†]	12 kbar[†]	12 kbar*	25 kbar*	37 kbar[†]
Al(1)–O$_A$ (x2)	1.827(3)	1.821(4)	1.821(3)	1.819(5)	1.815(3)
–O$_B$ (x2)	1.891(3)	1.891(4)	1.889(3)	1.888(5)	1.889(3)
–O$_D$ (x2)	2.086(2)	2.071(3)	2.070(2)	2.063(4)	2.045(3)
Avg.	1.935	1.928	1.927	1.923	1.916
Al(2)–O$_A$	1.816(4)	1.811(5)	1.811(4)	1.810(7)	1.808(5)
–O$_C$	1.839(4)	1.839(5)	1.833(4)	1.828(6)	1.826(4)
–O$_C$	1.899(4)	1.890(4)	1.894(3)	1.886(6)	1.875(4)
–O$_D$ (x2)	1.814(3)	1.811(4)	1.810(3)	1.806(5)	1.799(4)
Avg.	1.836	1.832	1.832	1.827	1.822
Si –O$_A$	1.645(4)	1.637(5)	1.640(4)	1.640(6)	1.633(4)
–O$_C$	1.618(4)	1.613(5)	1.612(4)	1.613(6)	1.617(4)
–O$_D$ (x2)	1.630(2)	1.622(4)	1.625(3)	1.620(5)	1.627(4)
Avg.	1.631	1.624	1.626	1.623	1.626

Bond Angles (°)	1 bar[†][1]	12 kbar†	12 kbar*	25 kbar*	37 kbar†
Al(1)–O$_D$–Al(2)	121.5(2)	121.5(2)	121.7(2)	121.6(3)	122.2(7)
Al(1)–O$_D$–Si	111.2(1)	111.3(2)	111.1(2)	111.1(3)	111.2(2)
Al(2)–O$_D$–Si	126.5(2)	126.4(1)	126.2(1)	126.3(2)	125.6(2)
O$_A$–Al(1)–O$_B$	96.5(1)	96.6(1)	96.7(1)	96.3(2)	96.5(1)
O$_D$–Al(1)–O$_A$	88.6(1)	88.3(2)	90.4(1)	89.0(2)	89.9(2)
O$_D$–Al(1)–O$_B$	91.6(7)	91.8(2)	91.6(2)	92.1(2)	92.1(2)
O$_B$–Si–O$_C$	101.3(2)	101.2(2)	101.3(2)	101.4(3)	101.2(2)
O$_D$–Si–O$_D$	109.3(1)	109.5(2)	109.1(2)	109.4(3)	109.1(3)
O$_D$–Si–O$_C$	111.4(1)	111.2(1)	111.5(1)	111.4(2)	111.4(1)
O$_A$–Al(2)–O$_C$	74.0(2)	74.0(2)	74.0(2)	74.2(3)	73.9(2)
O$_C$–Al(2)–O$_A$	86.7(2)	86.8(2)	86.8(1)	86.7(2)	87.3(2)
O$_D$–Al(2)–O$_A$	106.1(2)	106.2(2)	106.2(2)	106.3(3)	106.0(2)
O$_A$–Al(2)–O$_D$	99.1(1)	99.0(1)	99.2(1)	99.1(2)	99.4(1)
Al(2)–O–Si	123.7(2)	123.4(2)	123.8(2)	123.7(3)	123.3(2)
Al(2)–O–Al(2)	106.0(2)	106.0(2)	106.0(2)	105.8(3)	106.0(2)

† Continuous scan
* Step-scan

[1] From Winter and Ghose (1979).

which are 3, 3.8 and 7 mbar, respectively (Hazen and Finger, 1979). The octahedral bulk modulus of the AlO_6 octahedron in corundum, which is more compact and regular than that in andalusite, is 2.4±0.2 mbar (Finger and Hazen, 1978). The bulk modulus of the SiO_4 tetrahedron in diopside is 4 mbar (Levien and Prewitt, 1981). In quartz, however, where considerable bond bending is observed, the experimental SiO_4 tetrahedral bulk modulus is 7 mbar (Levien et al., 1980). The discrepancies in the experimental values of polyhedral bulk moduli and those predicted from linear bulk modulus–polyhedral volume relations may be explained by the fact that the first-approximation assumption of Hazen and Finger (1979) that all cation oxygen bonds have the same ionicity is invalid. In the case of andalusite, Iishi et al. (1979) have obtained best fit to the phonon spectra in their rigid-ion calculations by assuming the effective ionic charges for Al, Si and O to be 0.952, 0.476 and −0.476 respectively. On this basis, the Al–O bonds are considered to be 70% ionic. They did not distinguish between the effective ionic

charges of Al(1) and Al(2); in fact the Al(1)–O bonds should be slightly more ionic than the Al(2)–O bonds on the basis of average Al–O bond lengths within the Al(1) octahedron and the Al(2) trigonal bipyramid. The Si–O bond, on the other hand, was considered to be only 50% ionic (Pauling, 1960).

Lattice vibrations and soft modes

Phonon spectra of andalusite have been measured with polarized Raman and infrared spectroscopy and interpreted on the basis of a rigid-ion model by Iishi et al. (1979). From this study, Iishi et al. concluded that the dynamical structure of andalusite is given by rather rigid SiO_4 tetrahedra, linked together by much weaker and more ionic (70%) O–Al–O bonds. This conclusion is in accord with the high-temperature and high-pressure response of the andalusite structure as previously elaborated.

Iishi et al. (1979) have found that the ν_3 phonon modes, usually representing the totally symmetric stretching modes of a tetrahedron, are split in andalusite. Its high-energy branch, both in A and B_{1g} symmetry, has been assigned mainly to the stretching of the shortest Si–O (Si–O$_C$) bond, whereas the low-energy branch has been assigned to the stretching of the longest Si–O (Si–O$_B$) bond. If this assignment is correct, then at high pressure, where the Si–O$_B$ bond decreases significantly, one would predict the low-energy branch to increase in frequency.

Iishi et al. have also found that the Raman spectra of andalusite reveal two modes at 1,065 cm^{-1} (ν_{11}) and 242 cm^{-1} (ν_{114}) with a strong temperature dependence of their scattering frequencies. Both lines show A_{1g} symmetry; the temperature coefficients are both ca. 5.10^{-2} (cm^{-1}K^{-1}). The other A_{1g} modes at 553 cm^{-1} and 718 cm^{-1} shift with increasing temperature to lower values. These critical phonon branches show considerable contributions of the repulsive F1 force constant to their respective effective force constants. The potential term F1 is related to the nearest oxygen–oxygen distance (O$_C$–O$_C$) 2.247Å at room temperature. These edges lie in the **ab** plane and only phonons with normal coordinates predominantly parallel to these edges contribute to the critical behavior (Iishi et al., 1979).

If ν_{11} is correlated with the oxygen–oxygen interaction along the O$_C$–O$_C$ edge, it will soften at high temperature due to the increase (1.1% at 1000°C) in the O$_C$–O$_C$ edge length. This edge does not decrease significantly, however, at high pressure up to 37 kbar. Therefore, the high-pressure effect on the frequency of the ν_{11} will be negligible. The ν_{114} mode represents the rotation of the silicate tetrahedra, which may be caused by the increase of the Al(1)–O$_D$ bond length (or the O$_C$–O$_D$ edge of the Al(2)-polyhedron parallel to the **b**-axis) with temperature. At high pressure the Al(1)–O$_D$ bond length decreases considerably and the O$_C$–O$_D$ edge decreases by 3.7% at 37 kbar. Hence, if this assignment is correct, ν_{114} should increase in frequency at high pressure.

Anisotropic thermal vibrations

The shapes and orientations of the thermal vibration ellipsoids do not show any clear monotonic trends with pressure; however, the general nature of some of the vibrations can be discerned. The maximum vibration direction of Al(1) lies along the O_D–Al(1)–O_D bond axis; that of O_C is normal to the plane of Si and two Al(2) atoms bonded to it, and that of O_D in a plane normal to the line between Al(2) and Si atoms most closely bonded to it. It is clear that current techniques are not yet sufficiently precise, because of limited access to reciprocal space, to extract any but the most obvious information from anisotropic temperature factors refined from high-pressure data.

Conclusions

Although functional relationships among thermal expansion, compressibility and elasticity of andalusite have now been established, a more fundamental understanding of the thermodynamic behavior of andalusite will require a knowledge of the phonon dispersion relations as a function of pressure and temperature and the nature of chemical bonding. Certain conclusions, however, can be drawn based on this and previous studies:

1. The values of compressibility, thermal expansion and elasticity of andalusite are determined primarily by the more compliant Al(1) octahedron (particularly the long Al(1)–O_D bond) and secondarily, by the Al(2) trigonal bipyramid; the SiO_4 tetrahedron behaves like a rather rigid group.

2. The inverse relationship between pressure and temperature effects on the crystal structure of andalusite is only approximately correct. The deviation from this relationship may be the result of increased anharmonic thermal vibrations at high temperatures.

3. The softening of two phonon modes (ν_{11} 1,065 cm^{-1} and ν_{114} 242 cm^{-1}) with temperature (Iishi et al., 1979) can be correlated with the increase in two non-bonded oxygen–oxygen distances (respectively the O_C–O_C and O_C–O_D edges of the Al(2) trigonal bipyramid). With pressure the O_C–O_C edge does not change appreciably, whereas the O_C–O_D edge decreases by 3.7% at 37 kbar. Hence, with increase in pressure, the ν_{11} mode is predicted to be virtually unchanged, whereas the ν_{114} mode should increase in frequency.

References

Anderson, O. L. (1966). The use of ultrasonic measurement under modest pressure to estimate compression at high pressure. Journal of Physics and Chemistry of Solids, 27, 547–565.

Brace, W. F., Scholz, C. H., and La Mori, P. N. (1959). Isothermal Compressibility of kyanite, andalusite, and sillimanite from synthetic aggregates. Journal of Geophysical Research, 74, 2089–2098.

Burnham, C. W. and Buerger, M. J. (1961) Refinement of the crystal structure of andalusite. Zeitschrift für Kristallographie, 115, 269–290.

Cromer, D. T. and Liberman, D. (1970) Relativistic calculations of anomalous scattering factors for X-rays. Journal of Chemical Physics, 53, 1891–1898.

Cromer, D. T. and Mann, J. B. (1968) X-ray scattering factors computed from numerical Hartree-Fock wave functions. Acta Crystallographica, A24, 321–324.

Finger, L. W. and Hazen, R. M. (1978) Crystal structure and compression of ruby to 46 kbar. Journal of Applied Physics, 49, 5823–5826.

Finger, L. W. and Prince, E. (1975) A system of Fortran IV computer programs for crystal structure computations. National Bureau of Standards (United States) Technical Note, 854.

Hazen, R. M. (1977) Temperature, pressure and composition: structurally analagous variables. Physics and Chemistry of Minerals, 1, 83–94.

Hazen, R. M. and Finger, L. W. (1977) Modifications in high pressure single-crystal diamond-cell techniques. Carnegie Institution of Washington Year Book, 76, 655–656.

Hazen, R. M. and Finger, L. W. (1979) Bulk modulus-volume relationship for cation-anion polyhedra. Journal of Geophysical Research, 84, 6723–6728.

Hazen, R. M. and Finger, L. W. (1982) Comparative Crystal Chemistry. John Wiley and Sons, New York.

Iishi, K., Salje, E., and Werneke, C. (1979) Phonon spectra and rigid-ion model calculations on andalusite. Physics and chemistry of minerals, 4, 173–188.

King, H. E. and Finger, L. W. (1979) Diffracted beam crystal centering and its application to high-pressure crystallography. Journal of Applied Crystallography, 12, 374–378.

Lehman, M. A. and Larsen, F. K. (1974) A method for location of the peaks in step-scan-measured Bragg reflections. Acta Crystallographica A30, 580–584.

Levien, L. and Prewitt, C. T. (1981) High-pressure structural study of diopside. American Mineralogist, 66, 315–323.

Levien, L., Prewitt, C. T., and Weidner, D. J. (1980) Structure and elastic properties of quartz at pressure. American Mineralogist, 65, 920–930.

Merrill, L., and Basset, W. A. (1974) Miniature diamond anvil pressure cell for single crystal X-ray diffraction studies. Review of Scientific Instruments, 45, 290–294.

Pauling, L. (1960) The Nature of the Chemical Bond, 3rd Edition. Cornell University Press.

Taylor, W. H. (1929) The structure of andalusite. Zeitschrift für Kristallographie, 71, 205–218.

Vaughan, M. T. and Weidner, D. J. (1978) The relationship of elasticity and crystal structure in andalusite and sillimanite. Physics and Chemistry of Minerals, 3, 133–144.

Winter, J. K. and Ghose, S. (1979) Thermal expansion and high-temperature crystal chemistry of the Al_2SiO_5 polymorphs. American Mineralogist, 64, 573–586.